

# Controlling a diatomic shape resonance with non-resonant light

Ruzin Aĝanoĝlu,<sup>a</sup> Mikhail Lemeshko,<sup>b</sup> Bretislav Friedrich,<sup>b</sup> Rosario González-Férez,<sup>c</sup> Christiane P. Koch<sup>a,d</sup>

A (diatomic) shape resonance is a metastable state of a pair of colliding atoms quasi-bound by the centrifugal barrier imposed by the angular momentum involved in the collision. The temporary trapping of the atoms' scattering wavefunction corresponds to an enhanced atom pair density at low interatomic separations. This leads to larger overlap of the wavefunctions involved in a molecule formation process such as photoassociation, rendering the process more efficient. However, for an ensemble of atoms, the atom pair density will only be enhanced if the energy of the resonance comes close to the temperature of the atomic ensemble. Herein we explore the possibility of controlling the energy of a shape resonance by shifting it toward the temperature of atoms confined in a trap. The shifts are imparted by the interaction of non-resonant light with the anisotropic polarizability of the atom pair, which affects both the centrifugal barrier and the pair's rotational and vibrational levels. We find that at laser intensities of up to  $5 \times 10^9$  W/cm<sup>2</sup> the pair density is increased by one order of magnitude for <sup>87</sup>Rb atoms at 100  $\mu$ K and by two orders of magnitude for <sup>88</sup>Sr atoms at 20  $\mu$ K.

## 1 Introduction

The quest for translationally ultracold ( $T \leq 100 \mu\text{K}$ ) molecules in their absolute internal ground state has been rewarded recently when ultracold atoms were associated via a magnetic-field controlled Feshbach resonance followed by Stimulated Raman Adiabatic Passage.<sup>1,2</sup> Ultracold molecules were also produced by associating atoms using laser light<sup>3</sup> and brought into their rovibrational ground state by spontaneous or stimulated emission.<sup>4-6</sup> Feshbach or magneto-association requires non-zero nuclear spin – a hyperfine manifold – of the colliding atoms.<sup>7</sup> It is efficient when the collision energy of the atoms is of the order of the hyperfine splitting. This corresponds to nano-Kelvin temperatures which are reached via evaporative or sympathetic cooling, leaving typically only about  $10^4 - 10^5$  atoms that can be associated. Photoassociation<sup>3,8</sup> relies only on the presence of optical transitions which are usually abundant, and is not tied to any particular temperature regime (although the specific photoassociation mechanisms may differ at high<sup>9</sup> and very low<sup>8</sup> temperatures). In the ultracold domain, photoassociation has been often implemented in combination with magneto-optical traps (MOTs),<sup>8</sup> which hold up to  $10^{10}$  atoms at temperatures ranging between 10 – 100  $\mu$ K. However, only a small fraction of the MOT atoms are at internuclear separations,  $R$ , amenable to photoas-

sociation, i.e., the density of atom pairs within the required range of  $R$  is tiny. This reflects the fact that photoassociation cannot achieve the phase space compression required to transform far-apart atoms into tightly or even weakly bound molecules. As a result, the number of ground state molecules produced via photoassociation has been limited to only about  $10^4$ .<sup>5,6</sup>

A remedy for the limited efficiency of photoassociation could be found within the field of coherent control, which employs quantum interference to constructively enhance a desired outcome of a process while destructively suppressing all its undesirable alternatives.<sup>10,11</sup> Although coherent control has been successful for unimolecular processes such as photoionization or photodissociation,<sup>12,13</sup> controlling a binary reaction has remained an open challenge. This has been mainly due to the fact that the initial state of the reaction consists of an incoherent mixture of scattering states with random relative phases. However, resonances can, in principle, endow the mixture of the initial scattering states with a single phase.<sup>14</sup>

The way toward solving the problem of limited photoassociation efficiency may be paved by considering photoassociation as a coherent control problem. Coherent control employs quantum interference to constructively enhance a desired outcome of a process while destructively suppressing all its undesirable alternatives.<sup>10,11</sup> Although coherent control has been highly successful for unimolecular processes such as photoionization or photodissociation,<sup>12,13</sup> controlling a binary reaction such as photoassociation remains an open challenge. This is mainly due to the fact that the initial state of the reaction consists of an incoherent mixture of scattering states with random relative phases. However, resonances can, in principle, endow the mixture of the initial scattering states with a single phase.<sup>14</sup>

<sup>a</sup> Institut für Theoretische Physik, Freie Universität Berlin, Arnimallee 14, 14195 Berlin, Germany.

<sup>b</sup> Fritz-Haber-Institut der Max-Planck-Gesellschaft, Faradayweg 4-6, 14195 Berlin, Germany.

<sup>c</sup> Instituto Carlos I de Física Teórica y Computacional and Departamento de Física Atómica, Molecular y Nuclear, Universidad de Granada, 18071 Granada, Spain.

<sup>d</sup> Theoretische Physik, Universität Kassel, Heinrich-Plett-Str. 40, 34132 Kassel, Germany. Email: christiane.koch@uni-kassel.de

The importance of resonances increases in the ultracold regime where, along with tunneling, they dominate the quantum dynamics. The presence of a Feshbach resonance has been predicted to significantly enhance the photoassociation yield in Feshbach optimized photoassociation (FOPA).<sup>15</sup> Similarly, an enhanced microwave absorption is expected near a Feshbach resonance.<sup>16</sup> However, Feshbach enhancement of photoassociation is restricted to atoms with non-zero nuclear spin and is the more efficient the lower the temperature. Although electric field-induced resonances<sup>17–19</sup> should also increase the photoassociation efficiency, the electric fields required to achieve a significant enhancement are currently experimentally unfeasible. Shape resonances that occur when a scattering state becomes trapped behind the centrifugal barrier for partial waves with  $J > 0$  were found to yield enhanced photoassociation rates.<sup>20–22</sup> However, due to the rotational excitation involved in generating the barrier, the lowest energies at which shape resonances occur correspond typically to temperatures of a few milli-Kelvin. Therefore, the thermal weight of a shape resonance in a much colder MOT or optical trap is quite small.

Herein, we study the possibility of enhancing the thermal weight of a scattering resonance by shifting its position (with respect to the trap energy) by applying a non-resonant radiative field. The interaction of such a field with the anisotropic polarizability of the atom pair is of a universal character, independent of any particular energy level structure, frequency of the light (as long as it is non-resonant), or the presence of a permanent dipole moment. Non-resonant or far-off-resonant light was used to manipulate molecular alignment<sup>23–25</sup> and has been predicted to shift rotational and vibrational levels<sup>26</sup> or to modify intermolecular interactions<sup>27</sup>. It has also been predicted to cause peculiar effects in atomic Bose-Einstein condensates such as gravitational self-binding and supersolid-like structures.<sup>28–30</sup> The nonresonant polarizability interaction creates an effective rotational barrier for weakly bound molecules; and the subsequent ‘shaking’ of the molecules imparted by the nonresonant light could be employed to recover the vibrational probability density distribution of the corresponding bound atom pair.<sup>31,32</sup> The intuitive picture of an effective centrifugal barrier provided an impetus for the present study: if the non-resonant light creates (for  $J = 0$ ) or modifies (for  $J > 0$ ) the centrifugal barrier, it will also affect the position of a shape resonance. Application of a non-resonant field should therefore allow to control a shape resonance. The core of our present study extends the previous work on shifting weakly bound diatomic levels to shifting of quasi-bound scattering states.

The ubiquitous diatomic low- $J$  shape resonances are straightforward to predict from the basic scattering properties of ultracold atoms.<sup>22,33,34</sup> Specifically, we consider a  $d$ -wave shape resonance in 87-rubidium<sup>21</sup> and a  $g$ -wave shape reso-

nance in 88-strontium. Rubidium is the drosophila of ultracold physics, whose potential energy curves and polarizability anisotropy are accurately known. <sup>88</sup>Sr<sub>2</sub> features in proposals to test the time dependence of the electron-to-proton mass ratio.<sup>35</sup> With no Feshbach resonances present, <sup>88</sup>Sr<sub>2</sub> has been produced by photoassociation.<sup>36,37</sup> We compare the prospects for controlling the shape resonances of rubidium and strontium with non-resonant light and draw general conclusions about the applicability and efficiency of this control scheme for producing diatomics via photoassociation.

## 2 Theoretical framework

### 2.1 Description of a thermal cloud of atoms

The initial state of an ensemble of atoms held at thermal equilibrium in a trap of temperature  $T$  is described by the canonical density operator,

$$\hat{\rho}_{T,N} = \frac{1}{Z} e^{-\hat{\mathbf{H}}_N/k_B T}. \quad (1)$$

Equation (1) disregards the effects of quantum statistics, which are negligible at typical MOT temperatures. In a dilute gas where three-body and higher order interactions can be neglected, the Hamiltonian,  $\hat{\mathbf{H}}_N$ , consists only of single-particle ( $\hat{\mathbf{T}}, V_{\text{trap}}$ ) and two-body  $V_{ij}(\hat{\mathbf{R}}_{ij})$  operators. The  $N$ -particle density operator,  $\hat{\rho}_{T,N}$ , is then given in terms of  $N^2$ -times the pair density operator,  $\hat{\rho}_{T,2}$ .<sup>38</sup> Assuming that the center of mass and internuclear degrees of freedom can be separated – as is the case, e.g., in a harmonic trap – the center of mass motion can be integrated analytically. By representing the Hamiltonian for the internuclear motion on a finite-size coordinate-space grid with variables  $(R, \theta, \phi)$ , and making use of the azimuthal symmetry, the density matrix of the initial state can be constructed in terms of the eigenfunctions,  $\varphi_{nJ}(R, \theta)$ , of the pair Hamiltonian,  $\hat{\mathbf{H}}_2$ , with eigenvalues  $E_{nJ}$ ,<sup>38</sup>

$$\rho_{T,2}(R, \theta) = \frac{1}{4\pi R^2} \frac{\sum_{nJ} (2J+1) e^{-E_{nJ}/k_B T} |\varphi_{nJ}(R, \theta)|^2}{\sum_{nJ} (2J+1) e^{-E_{nJ}/k_B T}}. \quad (2)$$

The grid needs to be sufficiently large in  $R$  to approximate the scattering continuum well.<sup>39</sup> A small number of partial waves is sufficient to ensure convergence of the short-range part of  $\rho_{T,2}(R, \theta)$ , since only a few partial waves are thermally populated at very low temperatures.<sup>38</sup>

Formally, the time evolution of the cloud of atoms is determined by the dynamics of the pair density operator,

$$\hat{\rho}_{T,2}(t) = e^{-\frac{i}{\hbar} \hat{\mathbf{H}}_2 t} \hat{\rho}_{T,2}(t=0) e^{\frac{i}{\hbar} \hat{\mathbf{H}}_2 t}, \quad (3)$$

under the assumption that on the timescale of  $t$ , the time evolution is unitary, i.e., no dissipative mechanisms are present. Any thermal expectation value is obtained as  $\langle \hat{\mathbf{A}}(t) \rangle =$

$\text{Tr}[\hat{\mathbf{A}}\hat{\rho}_{T,2}(t)]$ . For example, the photoassociation probability is given by  $\langle \hat{\mathbf{P}}_e(t_f) \rangle$ , where  $\hat{\mathbf{P}}_e$  denotes the projector onto the electronic state  $e$  which is populated by photoassociation and  $t_f$  is some final time. The unitary time evolution in Eq. (3) implies that it is not necessary to solve the Liouville-von Neumann equation for the density operator explicitly. Rather, a separate propagation for each eigenstate in Eq. (2) is sufficient to calculate thermal expectation values.<sup>38</sup> In particular, if only the short range part of the initial thermal density is probed, only few partial waves suffice for convergence. This is numerically much more efficient than solving the Liouville-von Neumann equation since the number of terms in the sum of Eq. (2) is relatively small due to the narrow thermal width of an initial state at low temperature.

## 2.2 Interaction of a diatom with non-resonant laser light

The Hamiltonian of an atom pair in its electronic ground state in the presence of a non-resonant laser field can be written as

$$\hat{\mathbf{H}}_2^I = \hat{\mathbf{T}}_R + \frac{\hat{\mathbf{J}}^2}{2\mu\hat{\mathbf{R}}^2} + V_g(\hat{\mathbf{R}}) - \frac{2\pi I}{c} \left( \Delta\alpha(\hat{\mathbf{R}}) \cos^2 \hat{\theta} + \alpha_{\perp}(\hat{\mathbf{R}}) \right), \quad (4)$$

where the first and second terms denote the vibrational and rotational kinetic energies, respectively, and  $V_g(\hat{\mathbf{R}})$  the field-free ground electronic potential energy curve. The last term of Eq. (4) represents the interaction with a non-resonant laser field, with  $I$  the laser intensity and  $\Delta\alpha(\hat{\mathbf{R}}) = \alpha_{\parallel}(\hat{\mathbf{R}}) - \alpha_{\perp}(\hat{\mathbf{R}})$  the polarizability anisotropy, given in terms of the perpendicular and parallel molecular polarizability components,  $\alpha_{\perp}(\hat{\mathbf{R}})$  and  $\alpha_{\parallel}(\hat{\mathbf{R}})$ . For homonuclear dimers, the behaviour at large internuclear distances is given by Silberstein's expansion,<sup>40–43</sup>

$$\begin{aligned} \alpha_{\perp}(\hat{\mathbf{R}}) &\approx 2\alpha_0 - 2\alpha_0^2/\hat{\mathbf{R}}^3 + 2\alpha_0^3/\hat{\mathbf{R}}^6, \\ \alpha_{\parallel}(\hat{\mathbf{R}}) &\approx 2\alpha_0 + 4\alpha_0^2/\hat{\mathbf{R}}^3 + 8\alpha_0^3/\hat{\mathbf{R}}^6, \end{aligned} \quad (5)$$

where  $\alpha_0$  is the atomic polarizability. Hamiltonian (4) is derived by assuming the frequency of the laser to be far from any resonance and larger than the inverse of both the pulse duration and the rotational period. In this case, a two-photon rotating-wave approximation averaging over the rapid oscillations of the non-resonant field can be applied.<sup>44</sup> Furthermore, far from resonances, the frequency-dependent molecular polarizability approaches its static value, which allows to cast Eq. (4) in the static polarizability limit. The second-order nature of the light-matter interaction is reflected by the intensity (not the field amplitude) and  $\cos^2 \hat{\theta}$  operator occurring in the last term of Eq. (4). Thus the energy of the field-dressed eigenstates always decreases with increasing field intensity, i.e., the states are high-field seeking.

Since an external field defines a preferred direction in space, the symmetry of the corresponding Hamiltonian is reduced compared to the field-free case. In the absence of a field,

a bound molecular state is characterized by its vibrational, rotational, and magnetic quantum numbers  $(v, J, M)$ . This carries over to unbound box-discretized states approximating the scattering continuum above the dissociation limit, i.e.,  $(n, J, M)$  where each translational “quantum number” represents a range of scattering states with collisional energies close to  $E_n$ .<sup>38</sup> Due to the azimuthal symmetry about the laser polarization axis, the light-matter interaction depends only on the polar angle  $\theta$ . As a consequence, by turning on the non-resonant laser field, hybridization of the rotational motion takes place and only the magnetic quantum number  $M$  remains conserved. The field-free degeneracy of states with the same rotational quantum number  $J$  but different  $M$  is lifted due to the interaction with the laser field. Herein, we focus on states with  $M = 0$ , since for a given  $J$  the effect of the non-resonant field increases with decreasing  $M$  and is largest for  $M = 0$ . Thus, the sum in the density matrix (2) describing the initial state is restricted to states with  $M = 0$ , setting the degeneracy factor  $(2J + 1)$  to 1.

Discrete basis set methods are employed to represent the vibrational and rotational degrees of freedom of Hamiltonian (4). For the radial part, a mapped Fourier grid is used with the grid step set to be proportional to the local de Broglie wavelength.<sup>45–47</sup> This allows us to use large enough discretization boxes to properly describe the part of the scattering continuum that is relevant at ultracold temperatures. The rotational degree of freedom is treated by a discrete variable representation in terms of Legendre polynomials, taking into account that  $M$  is conserved.<sup>48,49</sup> At large intensities, more partial waves than those that are thermally populated initially will come into play, cf. Eq. (2). Convergence of our calculations with respect to the number of Legendre polynomials is ensured for the largest intensity employed ( $J_{max}^I \approx 14$  compared with  $J_{max}^0 = 3$  or 4 in the field-free case).

As evident from Eq. (4), the interaction with the non-resonant laser light couples  $\hat{\mathbf{R}}$  and  $\hat{\theta}$ , i.e., it affects both vibrational and rotational motion of the atom pair. In order to ease interpretation, it is expedient to disentangle the two effects by making use of effective one-dimensional models. The effect on the rotational motion is captured by an effective quantum number,  $J^*$ , determining the rotational barrier in an effective one-dimensional (vibrational) model.<sup>32</sup> If the non-resonant laser field is kept on, the effect of the field on the angular motion at a given internuclear separation needs to be accounted for by including the admixture of different partial waves and of the alignment. We therefore generalize previous treatments<sup>23,24,26,32,50,51</sup> to the latter case. In order to obtain an effective one-dimensional model in the presence of the non-resonant light, we first solve the angular part of the eigenvalue

problem for a fixed  $R$ ,

$$\left[ \frac{\hat{J}^2}{2\mu R^2} - \frac{2\pi I}{c} \left( \Delta\alpha(R) \cos^2 \hat{\theta} + \alpha_{\perp}(R) \right) \right] \Phi_j(\theta; R, I) = E_j(R, I) \Phi_j(\theta; R, I). \quad (6)$$

The eigenfunctions,  $\Phi_j(\theta; R, I)$ , and eigenvalues,  $E_j(R, I)$ , of this equation depend parametrically on the radial coordinate  $R$  and on the laser intensity  $I$ . The index  $j$  is a label which is related to the field-free rotational quantum number. The full wavefunction can be expanded in terms of these angular wavefunctions,

$$\Psi_{nJ}(R, \theta; I) = \sum_{j'} \psi_{nj'}(R; I) \Phi_{j'}(\theta; R, I). \quad (7)$$

Inserting this expansion into the time-independent Schrödinger equation for Hamiltonian (4), multiplying by  $\Phi_j^*(\theta; R)$ , integrating over the angular coordinate  $\theta$ , and neglecting all non-adiabatic coupling matrix elements,  $\int_0^\pi \Phi_j^*(\theta; R, I) \hat{\mathbf{T}}_R \Phi_{j'}(\theta; R, I) \sin \theta d\theta$ , the following effective one-dimensional Schrödinger equation for the vibrational part is obtained,

$$[\hat{\mathbf{T}}_R + V_g(\hat{\mathbf{R}}) + E_j(\hat{\mathbf{R}}; I)] \psi_{nj}(R; I) = E_n \psi_{nj}(R; I). \quad (8)$$

Here,  $V_g(R) + E_j(R; I)$  is the effective potential including the effect of non-resonant light. Note that although the index  $n$  is used as a label indicating a scattering state, this adiabatic model is also applicable to bound states. Figure 1 compares the field-free potential,  $V_g(R) + J(J+1)/(2\mu R^2)$  for  $J=2$ , with the effective potentials,  $V_g(R) + E_j(R; I)$ , for two intensities of the non-resonant field for  $^{87}\text{Rb}_2$ : as the field intensity increases, the height of the rotational barrier decreases.

Equation (8) represents an adiabatic approximation to the coupled rovibrational motion where the rotational wavefunction depends parametrically on the radial variable. This approximation is valid if the energy scales, or, respectively, timescales, associated with the rotational and vibrational motion are well separated. For very large field intensities, the adiabatic approximation is expected to break down, because the matter-field interaction becomes comparable to the vibrational energy scale. This allows for coupling between states in different vibrational bands which is neglected in Eq. (8).

### 2.3 Envisaged scheme for enhancement of photoassociation

Photoassociation in a magneto-optical trap can easily be saturated. Its efficiency is limited by the pair density at or near the Condon radius which is the internuclear distance where the photoassociation laser induces a resonant transition from the initial pair of colliding atoms to a weakly bound level

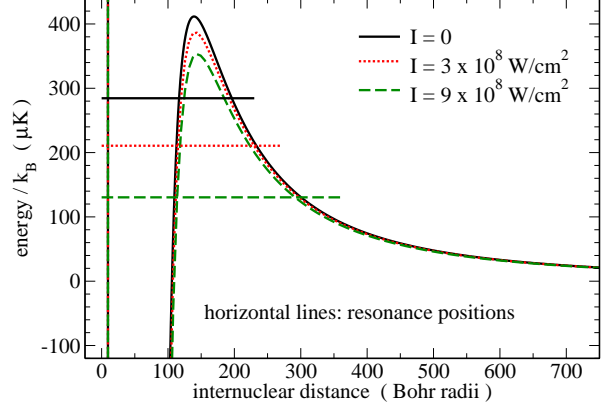


**Fig. 1** Effective potential,  $V_g(R) + E_j(R; I)$ , that the atom pair experiences in the presence of non-resonant laser light. The field-free rotational quantum number is  $J=2$  for which a shape resonance is observed at about  $290 \mu\text{K}$ . The non-resonant light shifts the position of the shape resonance to lower energies as indicated by the vertical lines (resonance positions calculated with the full  $2D$  Hamiltonian).

of the atoms' electronically excited state. The  $R$ -dependence of the pair density is given by  $\rho_{T,2}(R) = \int d\cos\theta \rho_{T,2}(R, \theta)$  and illustrated in Fig. 2 for  $^{87}\text{Rb}$  atoms. The constant behavior at large distances results from summing over many plane waves with random phases and reflects the equiprobability of finding two atoms at a certain distance. At short range, the interaction potential modulates the pair density. If only  $s$ -waves contribute significantly to the pair density, all scattering wave functions have their nodes at the same position at short range, giving rise to zeros in the pair density, cf.  $\rho_{T,2}(R)$  for  $T = 100 \mu\text{K}$  in Fig. 2. This reflects a threshold law<sup>52</sup> governing collisions at very low energy. Photoassociation occurs at intermediate distances, typically between  $40 a_0$  and  $200 a_0$  depending on the excited state potential curve. Such a choice of Condon radius is a compromise between large free-to-bound transition probabilities (demanding large  $R$ ) and sufficiently large binding energies required to avoid dissociation back into two atoms upon return to the electronic ground state (demanding short  $R$ ). If formation of molecules in their electronic ground state proceeds via a sequence of short, optimally chosen pump and dump pulses, integrated pulse energies on the order of a few nano-Joule are sufficient to completely deplete the pair density near the Condon radius.<sup>53</sup> Nevertheless, this creates only one to ten molecules per pulse sequence, depending on the density of the atoms in the trap.<sup>38</sup>

A further increase of the number of photoassociated molecules requires manipulation of the initial pair density,  $\rho_{T,2}(R)$ . To this end, we pursue the following idea for controlling a shape resonance with non-resonant light: A shape resonance is a quasi-bound state where the probability den-



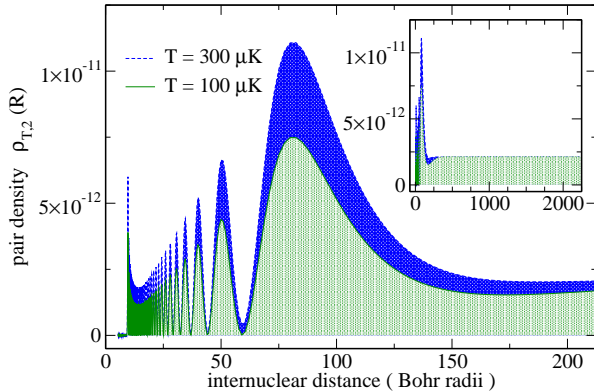


**Fig. 2** Thermal pair density  $\rho_{T,2}(R) = \int d\cos\theta \rho_{T,2}(R, \theta)$  for  $^{87}\text{Rb}$  atoms (without any non-resonant field): at long range, the probability of finding two atoms at a certain distance is equally distributed; at short range the interaction potential leads to a modulation of the pair density. For  $T = 300\ \mu\text{K}$ , the presence of the close-by  $d$ -wave shape resonance is reflected in an enhanced pair density at short range compared to  $T = 100\ \mu\text{K}$  and in the nodes of  $\rho_{T,2}(R)$  disappearing, for example near  $R = 58a_0$ , due to states with  $J > 0$ .

sity of an atom pair becomes trapped inside the rotational barrier. For typical detunings, this happens at distances that correspond to the Condon radius for photoassociation<sup>3,8</sup> and can therefore enhance the pair density that is available for excitation by a photoassociation laser. However, due to the thermal weight,  $e^{-E_{nj}/k_B T}$ , a shape resonance contributes significantly to the thermal ensemble described by Eq. (2) only if its energy is close to the thermal energy of the scattering atoms. However, the energy of shape resonances is usually of the order of milli-Kelvin, i.e., one to two orders of magnitude above typical MOT temperatures. We therefore apply non-resonant light with an intensity chosen such that the position of the shape resonance is moved toward the mean energy of the scattering atoms. One option consists in slowly switching on the non-resonant laser light, thereby ensuring adiabatic following of the thermal cloud of atoms. The field-free eigenstates present in the thermal density, Eq. (2), are then transformed adiabatically into field-dressed states, i.e., into the eigenstates of Hamiltonian (4). This modified density matrix, made up of the non-resonant field-dressed states, constitutes the initial state for photoassociation with short laser pulses.<sup>53–55</sup> Assuming that an optimally chosen photoassociation pulse completely depletes the modified pair density near the Condon radius – as in the field-free case<sup>53</sup> – the enhancement of the number of photoassociated molecules is simply given by the ratio of the field-dressed to the field-free thermal pair densities.

Short-pulse photoassociation under non-resonant field control involves two timescales: (i) a slow timescale for the switching of the non-resonant laser light, determined by the

requirement of adiabaticity with respect to the rotational motion, and (ii) a short timescale for the sequence of pump and dump pulses, determined by the requirement of a bandwidth that is optimal for photoassociation. The short timescale corresponds to a few picoseconds for transform-limited pulses (or a few tens of picoseconds for shaped pulses). The slow timescale is determined by the rotational periods which are found to be 82 ns and 36.5 ns for the rotational ground state of the last vibrational band for rubidium and strontium, respectively. While it is rather difficult to assign a rotational period to regular scattering states, the quasi-bound character of a shape resonance implies that its rotational period is well-defined. For the  $d$ -wave resonance of rubidium and the  $g$ -wave resonance of strontium considered below, we find rotational periods of  $2\ \mu\text{s}$  and 350 ns, respectively. A crucial question to be answered below is whether the modified shape resonances live long enough to allow for adiabatic switching of the non-resonant laser light.

### 3 Results and discussion

We study the non-resonant field control of a shape resonance for  $^{87}\text{Rb}$  and  $^{88}\text{Sr}$  at typical MOT temperatures, between  $50\ \mu\text{K}$  and  $150\ \mu\text{K}$  for rubidium and about  $20\ \mu\text{K}$  for strontium.<sup>37</sup> For colliding  $^{87}\text{Rb}$  atom pairs, a  $d$ -wave shape resonance has been observed at about  $290\ \mu\text{K}$ ,<sup>21</sup> and for  $^{88}\text{Sr}$ , we find a  $g$ -wave resonance at about 1.75 mK. Below, we investigate the influence of non-resonant laser light on the position and lifetime of these two shape resonances and the resulting enhancement of pair density at photoassociation distances. The feasibility of non-resonant field control of a shape resonance is determined by (i) the intensity required to move the position of the resonance close to energies corresponding to the MOT temperature and (ii) the lifetime of the modified resonance, which must be sufficiently long to enable adiabatic switching of the non-resonant field. The finite lifetime of the shape resonance is caused by tunneling through the rotational barrier of the quasi-bound resonance state. Following the intuitive picture suggested by Fig. 1, where the energy of the field-dressed shape resonance is plotted for two laser intensities, the lifetime of the resonance is expected to increase with the non-resonant field intensity.

Calculating resonance lifetimes at very low energies is a challenging numerical problem.<sup>56</sup> We have therefore employed two different methods to determine resonance lifetimes – complex absorbing potentials<sup>57</sup> and the width of peaks of the rotational constants,  $B_n = \langle n | \frac{1}{2\mu R^2} | n \rangle$ , that occur for shape resonances<sup>22</sup>. Complex absorbing potentials are characterized by two parameters, potential strength and width. Convergence with respect to these two parameters can be verified by representing the eigenvalues,  $(E_n, -i\Gamma_n/2)$ , in the complex

plane.<sup>57</sup> When the resonance occurs at very low energy, the potential strength needs to be small and the width huge, implying a very large spatial grid. Moreover, if the resonance is pushed below the dissociation threshold, the lifetime becomes infinite. As this limit is approached, it becomes increasingly difficult to achieve convergence of the parameters for the complex absorbing potential. When using the second method, the rotational constants,  $B_n = \langle n | \frac{1}{2\mu R^2} | n \rangle$ , are plotted versus energy,  $E_n$ , and fitted to a Lorentzian.<sup>22</sup> As the resonance position is shifted to lower energy by the non-resonant field, fewer box-discretized continuum states contribute to the peak such that identification of the peak becomes increasingly difficult. For all field intensities, the results agree with each other at least within 5%. This accuracy is sufficient for the order-of-magnitude estimate that is needed to determine the feasibility of the control scheme.

### 3.1 Rubidium

The potential energy curve for the lowest triplet state,  $a^3\Sigma_u^+$ , of  $^{87}\text{Rb}_2$ , is obtained by smoothly connecting *ab initio* data at short-range<sup>58</sup> with the asymptotic expansion  $C_6/R^6 + C_8/R^8 + C_{10}/R^{10}$  at long range where the  $C_i$  coefficients are taken from Ref. 59. Polarizabilities based on *ab initio* calculations are found in Ref. 60 and fit Silberstein's formula very well at distances larger than  $16a_0$ .<sup>\*</sup> Not surprisingly, the short-range behavior of the polarizabilities does not play any role in our study, i.e., calculations with the polarizabilities from Ref. 60 and calculations with polarizabilities according to Silberstein's expansion, Eq. (5), with some cutoff value at short distance give identical results.

Resonance energy and lifetime as a function of the non-resonant field intensity  $I$  are shown in Fig. 3 for the  $d$ -wave shape resonance of  $^{87}\text{Rb}$ , comparing the results of the  $2D$  description obtained by diagonalizing the Hamiltonian (4) with those obtained for the adiabatic model, Eq. (8). The position of the resonance is moved to smaller energies by increasing the field intensity, as expected. Overall, only moderate field intensities, smaller than  $10^9 \text{ W/cm}^2$ , are required to move the position of the resonance close to the energy that corresponds to a typical MOT temperature of  $100 \mu\text{K}$ . The adiabatic approximation underestimates the energy shift significantly for intensities larger than  $3 \times 10^8 \text{ W/cm}^2$ . We attribute this disagreement between the adiabatic approximation and the  $2D$  description to the fact that states belonging to different vibrational manifolds are mixed by a sufficiently strong non-resonant field. Such a mixing is not accounted for in the adiabatic approximation, cf. Section 2.2.

While the adiabatic approximation, Eq. (8) captures the qualitative behavior of the resonance energy as a function of

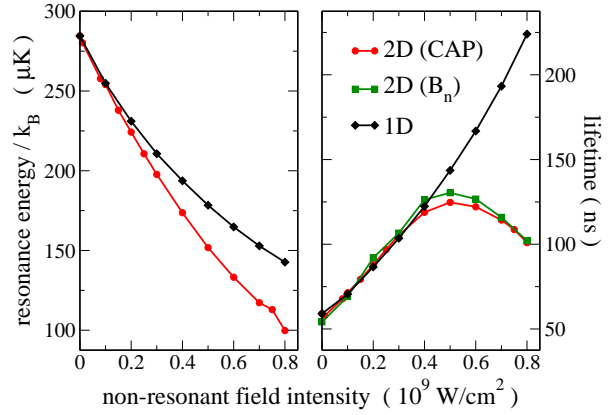


**Fig. 3** Energy and lifetime of the field-dressed shape resonance vs intensity of the non-resonant field for  $^{87}\text{Rb}$  (field-free  $d$ -wave shape resonance in the lowest triplet potential). Results for calculations based on the full  $2D$  Hamiltonian, Eq. (4), and the adiabatic approximation, Eq. (8), are compared. The lifetimes are calculated employing complex absorbing potentials (CAP,  $1D$  and  $2D$ ) and determining the peak width of the rotational constants ( $B_n$ ).

non-resonant field intensity correctly, its disagreement with the full  $2D$  description, Eq. (4), with respect to the lifetimes is striking for the large intensities shown in Fig. 3. In fact, such a dramatic breakdown of the adiabatic approximation is not necessarily expected since overall the intensities of Fig. 3 are moderate and one would expect a quantitative disagreement such as that found for the resonance energy. The adiabatic approximation essentially assumes that the effect of hybridization due to the non-resonant field is fully captured by the modified barrier height of effective potential, cf. Fig. 1; and it neglects in particular a coupling between rotational and vibrational motion. Vibrational motion that qualitatively differs for different rotational states is thus not correctly accounted for.

The degree of hybridization in the resonance wave function is examined in Fig. 4 by plotting the absolute square of the rotational weights,

$$c_J^I = \sum_n \int dR \int d\cos\theta \psi_{res}^{I*}(R, \theta) \phi_{nJ}(R, \theta),$$

for the lowest four even partial waves as a function of non-resonant field intensity (note that the coupling mixes only partial waves of the same parity). Here,  $\phi_{nJ}(R, \theta)$  denote the field-free eigenstates, i.e., the field-free box-quantized scattering states, and  $\psi_{res}^I(R, \theta)$  is the resonance wavefunction obtained by diagonalizing Hamiltonian (4) for a given value of the non-resonant field intensity  $I$ . For  $I = 0$ , the resonance is a pure  $J = 2$  state. As the non-resonant field intensity is increased, a substantial amount of  $J = 0$  is mixed in. Higher partial waves do not contribute to the resonance wavefunction (note the different scales of the  $J = 4$  and  $J = 6$  pan-

<sup>\*</sup>For  $R > 16a_0$ , the relative error is below 1% (3%) for the perpendicular (parallel) component.

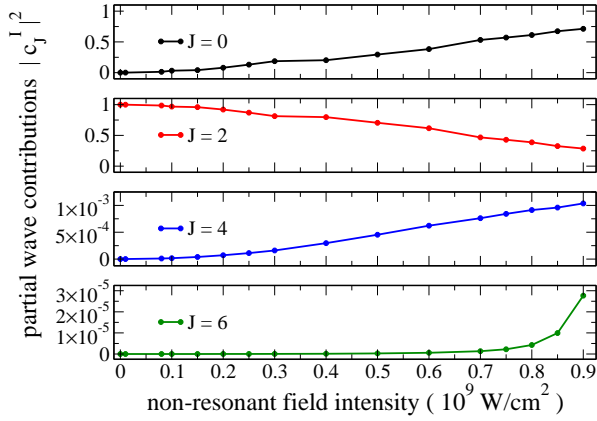


**Fig. 4** Contribution of different partial waves to the resonance wavefunction vs non-resonant field intensity for  $^{87}\text{Rb}$  (field-free  $J$ )

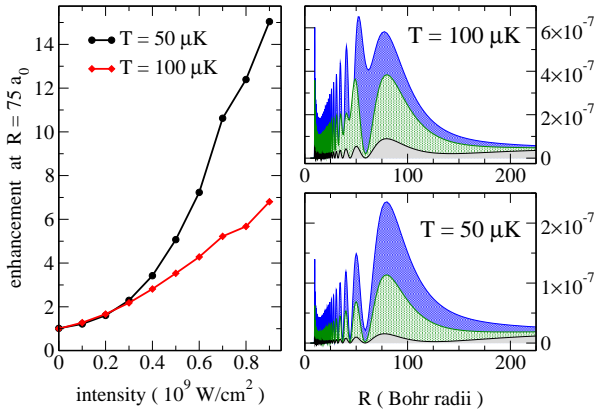


**Fig. 5** Modification of the rubidium pair density: Enhancement near  $R = 75 a_0$  (left) and  $R$ -dependence of the field-dressed pair density,  $\sum_{nJ} e^{-E_{nJ}/k_B T} \int d\cos\theta |\varphi_{nJ}(R, \theta)|^2 / 4\pi R^2$ , cf. Eq. (2), for zero field (grey),  $I = 6 \times 10^9 \text{ W/cm}^2$  (green) and  $I = 9 \times 10^9 \text{ W/cm}^2$  (blue).

els). A turnover in the resonance lifetime as a function of field intensity is observed in the right-hand side of Fig. 3. At the corresponding intensity, the  $J = 0$  contribution amounts to about 30%, and for the largest intensity shown in Fig. 4, the resonance wavefunction is predominantly of  $J = 0$  character. The different behavior of the lifetime in the full  $2D$  Hamiltonian and the adiabatic approximation is now easily rationalized by the qualitatively different  $R$ -dependences of the  $J = 2$  and  $J = 0$  states: While the field-free  $J = 2$  shape resonance is a quasi-bound state confined to short range by the centrifugal barrier, all  $J = 0$  states are of a purely scattering character. As the non-resonant field intensity is switched on, the resonance wavefunction becomes a superposition of these states, effectively loosing its quasi-bound character.

The effect of the non-resonant field on the pair density is

shown in Fig. 5. The pair density at photoassociation distances is enhanced by about one order of magnitude, cf. left-hand side of Fig. 5, due to increasing the thermal weight of the shape resonance by moving its energy close to  $k_B$  times the trap temperature. Nevertheless, the enhancement is larger for  $T = 50 \mu\text{K}$  compared to  $T = 100 \mu\text{K}$  although the resonance position is only moved to  $T = 100 \mu\text{K}$ , cf. Fig. 3 for the largest intensity shown in Fig. 5. This is due to the fact that for  $T = 100 \mu\text{K}$ , already the field-free pair density is influenced by the presence of the shape resonance, while its effect on the field-free pair density is negligible for  $T = 50 \mu\text{K}$ . The change brought about by the non-resonant field is thus larger for  $T = 50 \mu\text{K}$ . The enhancement of the pair density at all short distances is illustrated by the right-hand side of Fig. 5 which shows the  $R$ -dependence of the field-dressed pair density for three different intensities of the non-resonant field. The plotted quantity corresponds to the unnormalized pair density where the  $\theta$ -dependence has been integrated over. While a few partial waves are sufficient to converge the  $R$ -dependence of the pair density, the normalization factor requires a much larger number of partial waves for convergence.

The pair density is significantly enhanced also at distances shorter than the last peak of the last bound level. However, due to the fast oscillations of the wavefunction, this pair density enhancement does not translate into substantially larger number of molecules that can be photoassociated. The largest increase of the photoassociation efficiency is due to the pair density enhancement close to the last peak of the last bound level, i.e., about  $75 a_0$  for rubidium.

In summary, applying a non-resonant laser field shifts the position of the  $d$ -wave rubidium shape resonance to smaller energies. While this leads to an increasing lifetime of the resonance in an effective  $1D$  model, the shape resonance loses its quasi-bound character in the full  $2D$  description since it is mixed with states of pure scattering character. The lifetime therefore decreases after an initial increase. The rubidium atom pair density at distances relevant to photoassociation is found to increase by about one order of magnitude.

### 3.2 Strontium

The potential energy curve for the electronic ground state of  $^{88}\text{Sr}_2$  has been obtained spectroscopically, and an analytical fit was reported in Ref. 61. We approximate the polarizabilities by their long range expansion, Eq. (5), with the atomic values taken from Ref. 62.

Resonance energy and lifetime as a function of the nonresonant field intensity  $I$  are displayed in Fig. 6 for the  $g$ -wave shape resonance of  $^{88}\text{Sr}$ , comparing again results obtained for the  $2D$  Hamiltonian (4) with those of the adiabatic approximation, Eq. (8). Like in the case of rubidium, cf. Fig. 3, the position of the resonance is moved to smaller energies by in-

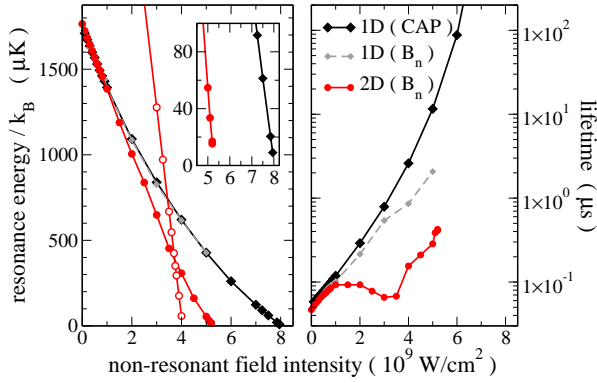


**Fig. 6** Energy and lifetime of the field-dressed shape resonance vs intensity of the non-resonant field for  $^{88}\text{Sr}$  (filled symbols: field-free  $g$ -wave ( $J = 4$ ) shape resonance in the electronic ground state potential, empty symbols: field-free  $J = 8$  resonance). Results for calculations based on the full  $2D$  Hamiltonian, Eq. (4), and the adiabatic approximation, Eq. (8), are compared. The lifetimes are calculated employing complex absorbing potentials (CAP,  $1D$ ) and determining the peak width of the rotational constants ( $B_n$ ,  $1D$  and  $2D$ ). Note the logarithmic scale for the lifetimes.

creasing the non-resonant field intensity. Slightly larger field intensities are required than for rubidium. This is easily rationalized in terms of the different atomic polarizabilities and rotational constants. The atomic polarizability of rubidium is larger than that of strontium, yielding a stronger interaction. Moreover, the rotational constant of strontium is larger than that of rubidium, so in order to achieve the same effect, a larger non-resonant field is required. Nevertheless, the intensities remain moderate for strontium as well: about  $5 \times 10^9 \text{ W/cm}^2$  are required to move the position of the resonance close to the energy corresponding to a MOT temperature of  $20 \mu\text{K}$ , typical for the two-color MOTs employed for alkaline-earth species.<sup>37</sup> Also, like for rubidium, the adiabatic approximation significantly underestimates the energy shift at the large laser intensities. This becomes particularly evident at intensities in excess of  $3 \times 10^9 \text{ W/cm}^2$ . Inspecting the pair density enhancement for strontium (see Fig. 8 below), a second resonant feature is observed which is attributed to a field-free  $J = 8$  shape resonance. The position of this resonance vs non-resonant field intensity is traced by empty red circles in Fig. 6. While the field-free  $J = 8$  resonance starts out at an energy much larger than that of the  $J = 4$  resonance, its energy is more strongly affected by the non-resonant field than that of the  $J = 4$  one. It is therefore moved to lower temperatures faster. The positions of the two resonances cross at about  $3.7 \times 10^9 \text{ W/cm}^2$ . Since both states have the same symmetry, the shape resonances exhibit an avoided crossing as  $I$  is varied. This field-induced phenomenon is characterized by a strong coupling between the vibrational and rotational mo-

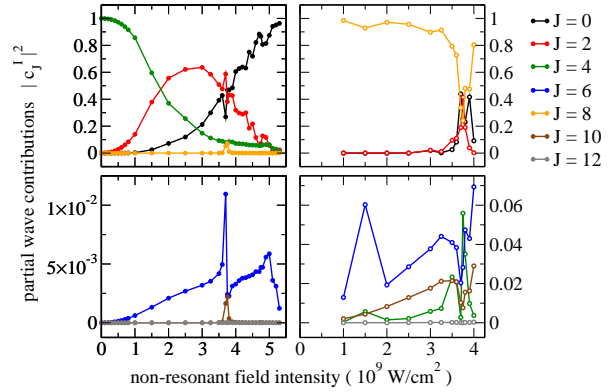


**Fig. 7** Contribution of different partial waves to the resonance wavefunction vs non-resonant field intensity for  $^{88}\text{Sr}$  (field-free  $J = 4$  shape resonance on the left-hand side, field-free  $J = 8$  shape resonance on the right-hand side).

tion.<sup>63</sup> It cannot be described by the adiabatic model which treats these two degrees of freedom as independent.

While for both rubidium and strontium the field-free lifetimes are on the order of  $50 \text{ ns}$ , a dramatic increase of the lifetime is observed for strontium as the non-resonant field is applied (note the logarithmic scale of the lifetimes on the right-hand ordinate in Fig. 6). This is in a stark contrast with rubidium, cf. Fig. 3, where an increasing lifetime is observed only in the adiabatic approximation, but was not confirmed by the  $2D$  calculation. In strontium, the  $2D$  lifetimes decrease with the non-resonant field intensity in an intermediate intensity range, but as the intensity is further increased, the lifetimes go up by an order of magnitude. The dip in the lifetimes, Fig. 6, occurs in a range of non-resonant field intensities where the  $J = 4$  and  $J = 8$  resonances are close in energy. Past the avoided crossing, the lifetime of the field-free  $J = 4$  resonance increases again due to the mixing that takes place in the crossing region: The  $J = 8$  resonance is quite narrow and thus long-lived. Due to the interaction of the two resonances, this character of the resonance is partially transferred to the field-free  $J = 4$  resonance. Despite the fact that both the adiabatic approximation and the  $2D$  description predict an overall increase of the lifetimes, the adiabatic approximation ceases to be valid for strontium (like for rubidium) at intermediate and large intensities since quantitatively both energies and lifetimes do not agree with those of the  $2D$  description: the more conservative estimates of the lifetime obtained in the adiabatic approximation by determining the peak width of the rotational constants are still an order of magnitude larger than the  $2D$  values. As for rubidium, the breakdown of the adiabatic approximation is attributed to mixing of states from different vibrational manifolds.

A mixing of states from different vibrational manifolds leads to particularly pronounced effects if two resonances



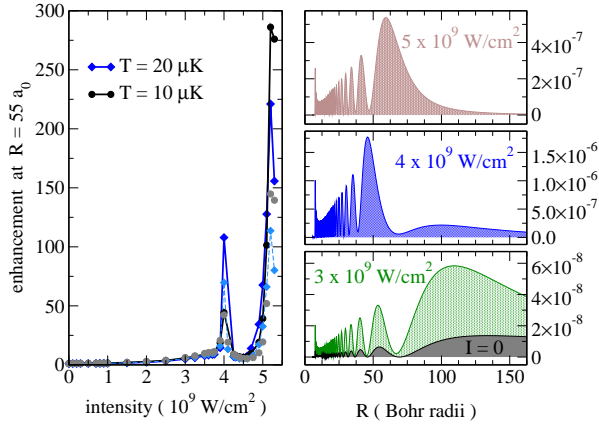


**Fig. 8** Modification of the strontium pair density: Enhancement near  $R = 55 a_0$  (left) and  $R$ -dependence of the field-dressed pair density,  $\sum_{n,J} e^{-E_{nJ}/k_B T} \int d \cos \theta |\varphi_{nJ}(R, \theta)|^2 / 4\pi R^2$ , cf. Eq. (2), for  $T = 20 \mu\text{K}$  (right). The lightblue and grey symbols in the left panel display the averaged enhancement (pair density integrated from  $R = 32 a_0$  to  $R = 120 a_0$ .) Note the different scales of the right-hand side panels.

are concerned, i.e., for non-resonant field intensities close to  $I = 3.7 \times 10^9 \text{ W/cm}^2$ , cf. left-hand side of Fig. 6. This is illustrated in Fig. 7 in terms of the partial contributions to the resonance wavefunctions for both the field-free  $J = 4$  resonance (left-hand side of Fig. 7) and the field-free  $J = 8$  shape resonance (right-hand side of Fig. 7). For  $I = 0$ , the resonance wavefunctions are pure  $J = 4$  and  $J = 8$  states, respectively. As the non-resonant field is switched on, a substantial amount of first  $J = 2$  and then  $J = 0$  is mixed in to the field-free  $J = 4$  state. While this resonance wavefunction is predominantly of  $J = 2$  character at intermediate intensities, it acquires essentially an  $s$ -wave character at large intensities. Close to the intensity where the two resonances cross, some  $J = 8$  character is mixed in as well (little orange peak in the left-hand side of Fig. 7). The presence of the second resonance shows up in all the partial wave contributions causing discontinuous behavior near the crossing point. Partial waves corresponding to  $J = 10$  and higher do not contribute to the resonance wavefunctions (grey symbols in the left-hand side of Fig. 7). The field-free  $J = 8$  shape resonance (right-hand side of Fig. 7) essentially keeps its character with just a small admixture of  $J = 6$  until the crossing region with the  $J = 4$  resonance is reached. There it acquires a substantial amount of  $J = 2$  and  $J = 0$  character. This is due to the strong mixing between both states induced by the avoided crossing. Once the crossing region is passed, the resonance wavefunction recovers its mainly  $J = 8$  character. This represents another unambiguous signature of interaction between the two resonances.

The presence of the two resonances shows up clearly also in the modification of the pair density, cf. Fig. 8. While the

first peak in the enhancement (left-hand side of Fig. 8), near  $I = 4 \times 10^9 \text{ W/cm}^2$ , is due to the field-free  $J = 8$  resonance whose energy approaches that corresponding to the trap temperature, the second peak, near  $I = 5 \times 10^9 \text{ W/cm}^2$ , can be attributed to the field-free  $J = 4$  resonance. Unlike rubidium, where the nodal structure of the pair density was only slightly modified by shifting down the resonance, cf. Fig. 5, the  $R$ -dependence of the pair density depends sensitively on the non-resonant field intensity, cf. right-hand side of Fig. 8. The enhancement at a specific position is therefore compared to an averaged enhancement obtained by integrating the pair density in all relevant photoassociation distances, from  $R = 32 a_0$  to  $R = 120 a_0$  (light-blue and grey symbols in the left-hand side of Fig. 8). The overall trend and order of magnitude behavior of the averaged enhancement is the same as the enhancement at a specific distance,  $R = 55 a_0$ . The sensitive  $R$ -dependence of the pair density on laser intensity reflects the contribution of the two resonances which, in an effective description, correspond to two different centrifugal barriers with different turning points. It is the outer turning point at each of the centrifugal barriers that causes the large peaks near  $R = 45 a_0$  for  $I = 4 \times 10^9 \text{ W/cm}^2$  and near  $R = 60 a_0$  for  $I = 5 \times 10^9 \text{ W/cm}^2$ . Note that the pair density is also enhanced at the laser intensities where the two resonances exhibit the avoided crossing,  $I = 3.75 \times 10^9 \text{ W/cm}^2$ . However, the effect is most visible for a temperature around  $T = 200 \mu\text{K}$ , which is much larger than typical strontium MOT temperatures.

In summary, the interaction of two resonances leaves a pronounced signature in the atom pair density, one that should be observable in an experiment which probes the pair density.<sup>64</sup> Moreover, for zero-field resonances which are far from the trap temperature, a large enhancement of the atom pair density – here about 2 orders of magnitude – and an increase in the field-free resonance lifetime are found.

We note that an enhanced pair density at photoassociation internuclear separations brought about by tuning a shape resonance could also enable photoassociation based on Stimulated Raman Adiabatic Passage (STIRAP)<sup>65</sup> either within a single pair of pump and Stokes pulses or within a sequence of phase-locked STIRAP pulse pairs.<sup>66,67</sup> The feasibility of STIRAP photoassociation depends on a sufficient isolation of the initial state from the scattering continuum. A possibility to achieve this discussed in the literature is based on utilizing a Feshbach resonance.<sup>68</sup> If, however, no resonance is present, i.e., for an unstructured continuum, STIRAP fails. Therefore, experiments that made use of STIRAP for transferring molecules to their ground state started from molecules that had been already associated via a Feshbach resonance.<sup>1,2,69,70</sup> A shape resonance that is brought to the right energy by non-resonant laser light might provide an alternative way to isolate the initial state for STIRAP from the scattering continuum. It would not rely on the presence of Feshbach resonances which

---

do not occur for example for the even isotope species of alkaline earth atoms.<sup>7</sup> However, STIRAP induces a second slow timescale, due to the requirement of adiabaticity with respect to the initial state. This translates into an even longer lifetime of the shape resonance that is required to guarantee success of STIRAP photoassociation compared with the non-adiabatic picosecond pump-dump photoassociation sequence discussed above.

## 4 Conclusions

We have considered the interaction of non-resonant laser light with pairs of colliding atoms held in a magneto-optical trap, employing a rigorous treatment of the thermal ensemble of atoms and comparing a  $2D$  description of the coupled rovibrational motion to an effective  $1D$  model based on the adiabatic approximation. Specifically, we have studied the influence of the non-resonant light on the position and the lifetime of shape resonances. Such quasi-bound states, that are trapped behind the centrifugal barrier imposed by the angular momentum involved in the collision, lead to significant enhancement of the pair density at comparatively short range. This enhancement readily translates into an increased efficiency of molecule-formation processes such as photoassociation.<sup>20,21</sup> Since the photoassociation rate is limited by the pair density at or near the Condon radius,<sup>38,53</sup> utilizing shape resonances could overcome the main obstacle toward forming large numbers of molecules.

However, most of the time, the thermal weight of shape resonances at MOT temperatures is very small because their energy is too high. In the present study, we find that the energy of shape resonances can be decreased over several orders of magnitude by applying a non-resonant laser field. It is the second order nature of the laser-matter interaction that guarantees a monotonous decrease in energy. Moderate intensities of the non-resonant field are sufficient: intensities of less than  $10^9 \text{ W/cm}^2$  are required to move the  $d$ -wave resonance of rubidium from  $300 \mu\text{K}$  to below  $100 \mu\text{K}$ , and intensities of about  $5 \times 10^9 \text{ W/cm}^2$  shift the  $g$ -wave resonance of strontium from  $1.75 \text{ mK}$  to below  $20 \mu\text{K}$ . The value of the required non-resonant field intensity is determined by the rotational constant and the atomic polarizability of a given species: small rotational constants and large polarizabilities are desirable to maximize the matter-field interaction and minimize the (competing) rotational kinetic energy.

As the non-resonant field intensity is increased, the lifetime of a shape resonance first increases, then drops again. We rationalize the increase within the  $1D$  picture by the increase in the tunneling time through the centrifugal barrier which accompanies the lowering of the energy of the resonance. However, the  $1D$  picture captures only part of the story: as the field intensity is further increased, strong hybridization occurs. As

scattering states belonging to different partial waves get mixed in, the resonance wavefunction loses its quasi-bound character, whereby tunneling out of the centrifugal barrier is actually enhanced. This is the generic behavior of an isolated shape resonance which is observed in our example of the  $J = 2$  resonance in rubidium. A  $2D$  description of the coupled rovibrational motion is essential to capturing this effect correctly even for comparatively moderate intensities. The adiabatic approximation, which assumes the vibrational and rotational degrees of freedom to be independent for all states, ceases to be valid.

The physical situation changes once more if more than one resonance comes into play, as in our example of strontium where a broad  $J = 4$  resonance and a narrow  $J = 8$  resonance interact. For strong fields, the two resonances show an avoided crossing, in the course of which part of the narrow-resonance character of the  $J = 8$  resonance is transferred to the  $J = 4$  resonance, increasing the lifetime of the latter. Of course, the interaction of different resonances also requires a  $2D$  description of the coupled rovibrational motion and is not accounted for in an effective  $1D$  treatment.

For both single and interacting resonances, significant enhancement of the thermal pair density at short distances is found. The magnitude of the enhancement depends on the distance between the field-free resonance position and the trap temperature. Maximum enhancement is obtained when the non-resonant field intensity is chosen such that the position of the shape resonance matches the trap temperature. In our examples, an enhancement on the order of 10 and 100 was found for rubidium and strontium, respectively. Such an enhancement can be probed directly by pulses that are short on the timescale of the rotational and translational motion in the trap, for example by picosecond pulses.<sup>64</sup>

Our thermally averaged pair densities describe the structure of the rovibrational eigenvalue problem for a given non-resonant field intensity. This gives rise to both a dynamic and a static regime that can be pursued to implement non-resonant field control of shape resonances in an experiment. The dynamic regime consists of applying a non-resonant laser pulse which is long compared with the rotational motion associated with the shape resonance. The shape resonance adiabatically follows the pulse and is shifted toward lower energies. Once the energy corresponding to the trap temperature is reached, a resonant photoassociation or probe pulse is applied that is short with respect to the non-resonant laser pulse. This scheme is expected to be successful if the timescale of the adiabatic switching is of the order of the lifetime of the resonance or shorter. In our study, we found rotational periods of  $2 \mu\text{s}$  and lifetimes of up to  $100 \text{ ns}$  for rubidium, whereas for strontium we found rotational periods of  $350 \text{ ns}$  and lifetimes of  $500 \text{ ns}$ . Therefore, adiabatic following cannot be ensured for rubidium. While losses due to the lifetime of the resonance might hamper the realization of a full two-orders-

of-magnitude enhancement, the enhancement found for strontium is significant. In general, controlling a shape resonance with non-resonant laser light based on adiabatic following will be successful for species with short rotational periods (or large rotational constants).

As an alternative to adiabatically shifting the position of a shape resonance, a static scheme can be pursued. This is based on the fact that the thermally averaged atom pair density describes a thermal equilibrium in the trap for a given temperature and non-resonant field intensity. The static scheme involves application of a constant non-resonant field and a hold period for thermalization of the atom cloud in the presence of the field. The field-modified equilibrium can then serve as a starting point for photoassociation, using either continuous-wave lasers or laser pulses.

Finally, we wish to point out that our approach differs from previous studies on the resonance-enhancement of the short-range pair density and the subsequent molecule formation<sup>15–19</sup> in that we seek to *actively* control the resonance. This is in contrast to the literature which discusses the influence of a given resonance on the desired process, e.g., molecule formation. Following the spirit of coherent control where resonances can be used to imprint a well-defined phase onto the initial state of the desired process,<sup>14</sup> in our present study the resonance itself is the subject of control, in order to afford an optimal use of it. In terms of controllability, our main finding is that shape resonances can be controlled in their energetic position but not at the same time in their vibrational character (purely scattering vs quasi-bound). This insight defines the challenge for future work – to identify a fully controllable scattering resonance.

## Acknowledgments

Financial support from the Deutsche Forschungsgemeinschaft (Grant No. KO 2301/2), by the Spanish project FIS2008-02380 (MICINN) as well as the Grants FQM-2445 and FQM-4643 (Junta de Andalucía), Campus de Excelencia Internacional Proyecto GENIL CEB09-0010 is gratefully acknowledged. RGF belongs to the Andalusian research group FQM-207. BF and ML thank Gerard Meijer for discussions and support.

## References

- 1 K.-K. Ni, S. Ospelkaus, M. H. G. de Miranda, A. Pe'er, B. Neyenhuis, J. J. Zirbel, S. Kotochigova, P. S. Julienne, D. S. Jin and J. Ye, *Science*, 2008, **322**, 231.
- 2 J. G. Danzl, E. Haller, M. Gustavsson, M. J. Mark, R. Hart, N. Bouloufa, O. Dulieu, H. Ritsch and H.-C. Nägerl, *Science*, 2008, **321**, 1062.
- 3 K. M. Jones, E. Tiesinga, P. D. Lett and P. S. Julienne, *Rev. Mod. Phys.*, 2006, **78**, 483.
- 4 J. M. Sage, S. Sainis, T. Bergeman and D. DeMille, *Phys. Rev. Lett.*, 2005, **94**, 203001.
- 5 J. Deiglmayr, A. Grochola, M. Repp, K. Mörtlbauer, C. Glück, J. Lange, O. Dulieu, R. Wester and M. Weidemüller, *Phys. Rev. Lett.*, 2008, **101**, 133004.
- 6 M. Viteau, A. Chotia, M. Allegrini, N. Bouloufa, O. Dulieu, D. Comparat and P. Pillet, *Science*, 2008, **321**, 232.
- 7 T. Köhler, K. Góral and P. S. Julienne, *Rev. Mod. Phys.*, 2006, **78**, 1311.
- 8 F. Masnou-Seeuws and P. Pillet, *Adv. in At., Mol. and Opt. Phys.*, 2001, **47**, 53.
- 9 U. Marvet and M. Dantus, *Chem. Phys. Lett.*, 1995, **245**, 393.
- 10 S. A. Rice and M. Zhao, *Optical control of molecular dynamics*, John Wiley & Sons, 2000.
- 11 P. Brumer and M. Shapiro, *Principles and Applications of the Quantum Control of Molecular Processes*, Wiley Interscience, 2003.
- 12 H. Rabitz, R. de Vivie-Riedle, M. Motzkus and K. Kompa, *Science*, 2000, **288**, 824.
- 13 *Analysis and control of ultrafast photoinduced reactions*, ed. O. Kühn and L. Wöste, Springer, Berlin, 2007.
- 14 V. Zeman, M. Shapiro and P. Brumer, *Phys. Rev. Lett.*, 2004, **92**, 133204.
- 15 P. Pellegrini, M. Gacesa and R. Côté, *Phys. Rev. Lett.*, 2008, **101**, 053201.
- 16 S. V. Alyabyshev and R. V. Krems, *Phys. Rev. A*, 2010, **82**, 030702.
- 17 R. V. Krems, *Phys. Rev. Lett.*, 2006, **96**, 123202.
- 18 R. González-Férez and P. Schmelcher, *New J. Phys.*, 2009, **11**, 055013.
- 19 D. Chakraborty, J. Hazra and B. Deb, *J. Phys. B*, 2011, **44**, 095201.
- 20 H. M. J. M. Boesten, C. C. Tsai, B. J. Verhaar and D. J. Heinzen, *Phys. Rev. Lett.*, 1996, **77**, 5194.
- 21 H. M. J. M. Boesten, C. C. Tsai, J. R. Gardner, D. J. Heinzen and B. J. Verhaar, *Phys. Rev. A*, 1997, **55**, 636.
- 22 B. E. Londoño, J. E. Mahecha, E. Luc-Koenig and A. Crubellier, *Phys. Rev. A*, 2010, **82**, 012510.
- 23 B. Friedrich and D. Herschbach, *Phys. Rev. Lett.*, 1995, **74**, 4623.
- 24 B. Friedrich and D. Herschbach, *J. Phys. Chem.*, 1995, **99**, 15686.
- 25 H. Stapelfeldt and T. Seideman, *Rev. Mod. Phys.*, 2003, **75**, 543.
- 26 M. Leshchko and B. Friedrich, *J. Phys. Chem. A*, 2010, **114**, 9848.
- 27 M. Leshchko, *arXiv:1104.1046*.
- 28 D. O'Dell, S. Giovanazzi, G. Kurizki and V. M. Akulin, *Phys. Rev. Lett.*, 2000, **84**, 5687.
- 29 S. Giovanazzi, D. O'Dell and G. Kurizki, *Phys. Rev. Lett.*, 2002, **88**, 130402.
- 30 D. H. J. O'Dell, S. Giovanazzi and G. Kurizki, *Phys. Rev. Lett.*, 2003, **90**, 110402.
- 31 B. Friedrich, M. Gupta and D. Herschbach, *Coll. Czech Chem. Commun.*, 1998, **63**, 1089.
- 32 M. Leshchko and B. Friedrich, *Phys. Rev. Lett.*, 2009, **103**, 053003.
- 33 B. Gao, *Phys. Rev. A*, 1998, **58**, 4222.
- 34 B. Gao, *Phys. Rev. A*, 2009, **80**, 012702.
- 35 T. Zelevinsky, S. Kotochigova and J. Ye, *Phys. Rev. Lett.*, 2008, **100**, 043201.
- 36 S. B. Nagel, P. G. Mickelson, A. D. Saenz, Y. N. Martinez, Y. C. Chen, T. C. Killian, P. Pellegrini and R. Coté, *Phys. Rev. Lett.*, 2005, **94**, 083004.
- 37 T. Zelevinsky, M. M. Boyd, A. D. Ludlow, T. Ido, J. Ye, R. Ciuryło, P. Naidon and P. S. Julienne, *Phys. Rev. Lett.*, 2006, **96**, 203201.
- 38 C. P. Koch, R. Kosloff, E. Luc-Koenig, F. Masnou-Seeuws and A. Crubellier, *J. Phys. B*, 2006, **39**, S1017.
- 39 E. Luc-Koenig, R. Kosloff, F. Masnou-Seeuws and M. Vatasescu, *Phys. Rev. A*, 2004, **70**, 033414.
- 40 L. Silberstein, *Philos. Mag.*, 1917, **33**, 92.
- 41 L. Silberstein, *Philos. Mag.*, 1917, **33**, 215.
- 42 L. Silberstein, *Philos. Mag.*, 1917, **33**, 521.
- 43 L. Jensen, P.-O. Åstrand, A. Osted, J. Kongsted and K. V. Mikkelsen, *J.*

- 
- Chem. Phys.*, 2002, **116**, 4001.
- 44 P. S. Pershan, J. P. van der Ziel and L. D. Malmstrom, *Phys. Rev.*, 1966, **143**, 574.
- 45 V. Kokoouline, O. Dulieu, R. Kosloff and F. Masnou-Seeuws, *J. Chem. Phys.*, 1999, **110**, 9865.
- 46 K. Willner, O. Dulieu and F. Masnou-Seeuws, *J. Chem. Phys.*, 2004, **120**, 548.
- 47 S. Kallush and R. Kosloff, *Chem. Phys. Lett.*, 2006, **433**, 221.
- 48 Z. Bačić and J. C. Light, *Annu. Rev. Phys. Chem.*, 1989, **40**, 469.
- 49 J. C. Light and T. Carrington, *Adv. Chem. Phys.*, 2000, **114**, 263.
- 50 R. González-Férez and P. Schmelcher, *Phys. Rev. A*, 2004, **69**, 023402.
- 51 R. González-Férez and P. Schmelcher, *Phys. Rev. A*, 2005, **71**, 033416.
- 52 A. Crubellier and E. Luc-Koenig, *J. Phys. B*, 2006, **39**, 1417.
- 53 C. P. Koch, R. Kosloff and F. Masnou-Seeuws, *Phys. Rev. A*, 2006, **73**, 043409.
- 54 C. P. Koch, E. Luc-Koenig and F. Masnou-Seeuws, *Phys. Rev. A*, 2006, **73**, 033408.
- 55 C. P. Koch and R. Moszyński, *Phys. Rev. A*, 2008, **78**, 043417.
- 56 J. Muga, J. Palao, B. Navarro and I. Egusquiza, *Phys. Rep.*, 2004, **395**, 357.
- 57 U. V. Riss and H.-D. Meyer, *J. Phys. B*, 1993, **26**, 4503.
- 58 S. J. Park, S. W. Suh, Y. S. Lee and G.-H. Jeung, *J. Molec. Spec.*, 2001, **207**, 129.
- 59 A. Marte, T. Volz, J. Schuster, S. Dürr, G. Rempe, E. G. M. van Kempen and B. J. Verhaar, *Phys. Rev. Lett.*, 2002, **89**, 283202.
- 60 J. Deiglmayr, M. Aymar, R. Wester, M. Weidemüller and O. Dulieu, *J. Chem. Phys.*, 2008, **129**, 064309.
- 61 A. Stein, H. Knöckel and E. Tiemann, *Phys. Rev. A*, 2008, **78**, 042508.
- 62 *CRC handbook of chemistry and physics*, ed. D. R. Lide, Taylor and Francis, 91st edn., 2009.
- 63 R. González-Férez and P. Schmelcher, *Europhys. Lett.*, 2005, **72**, 555.
- 64 C. P. Koch and R. Kosloff, *Phys. Rev. Lett.*, 2009, **103**, 260401.
- 65 K. Bergmann, H. Theuer and B. W. Shore, *Rev. Mod. Phys.*, 1998, **70**, 1003.
- 66 E. A. Shapiro, M. Shapiro, A. Pe'er and J. Ye, *Phys. Rev. A*, 2007, **75**, 013405.
- 67 E. A. Shapiro, A. Pe'er, J. Ye and M. Shapiro, *Phys. Rev. Lett.*, 2008, **101**, 023601.
- 68 E. Kuznetsova, M. Gacesa, P. Pellegrini, S. F. Yelin and R. Côté, *New J. Phys.*, 2009, **11**, 055028.
- 69 F. Lang, K. Winkler, C. Strauss, R. Grimm and J. H. Denschlag, *Phys. Rev. Lett.*, 2008, **101**, 133005.
- 70 S. Ospelkaus, A. Pe'er, K.-K. Ni, J. J. Zirbel, B. Neyenhuis, S. Kotochigova, P. S. Julienne, J. Ye and D. S. Jin, *Nature Phys.*, 2008, **4**, 622.